Research Article
doi.org/10.1002/anse.202200006

Chemistry Europe
European Chemical Societies Publishing

www.analysis-sensing.org

Multimodal Imaging of Silicified Sorghum Leaves

Victor M. R. Zancajo,[a, b, c] Sabrina Diehn,[b] Rivka Elbaum,[a, d] and Janina Kneipp*[a, b, c]

The plant cell wall is a complex composite material made of polysaccharides, polyphenols, proteins, and minerals. In this work, a multimodal imaging approach was taken, using Raman and Fourier-transform infrared (FTIR) microspectroscopy along with fluorescence imaging, scanning electron microscopy (SEM), and elemental mapping by energy dispersive X-ray spectroscopy (EDX). We characterized the chemical composition of sorghum leaf cross-sections extracted from fresh tissue as well as after paraffin embedding. The complementary vibrational information of Raman and FTIR spectra related a silica deposition to a specific organic composition in the epidermis, specifically with respect to lignin. Moreover, the data enable in situ correlation of autofluorescence with a specific lignin structure. Our results showed that lignin 5–5′ linkages that produce biphenyl structures are important determinants of the cell wall fluorescence properties. The reported multimodal approach will help to clarify the process of biosilica formation and related questions regarding cell wall biochemistry.

Introduction

The cell walls of plant tissues are complex composite materials consisting of the organic macromolecules cellulose, lignin, and hemicelluloses. The tissues of plants are categorized into three systems, according to their function: the epidermis, the ground tissue that includes sclerenchyma and parenchyma (bundle sheath), and the vascular tissue comprised of phloem and xylem, (see Figure 1), with their function determining the specific structure and composition of their cell walls.[1] In addition to the cell wall polymers, inorganic components can be deposited in specific plant organs.[2] Plant mineralization is common, especially the deposition of silica that forms microscopic structures called phytoliths. The presence of silica greatly influences the mechanical properties of the cell walls[2] and also confers numerous and well documented benefits to the plants.[3] They include protection against biotic stresses such as virus infection, molds, and bacteria and abiotic stress such as resistance to drought, extreme temperatures or toxic compounds,[4] yet the mechanisms are not clear.[5] The organic compounds that are responsible for the silica deposition and the influence of the organic matrix on the precipitation of silica are not completely understood[6] but can be studied with the help of spectroscopic tools, as shown by us in previous work.[7] By characterizing the biomolecular matrix in a plant tissue, those organic components that play a key role in silicification may become identified, and their particular function can be elucidated subsequently in mechanistic studies.

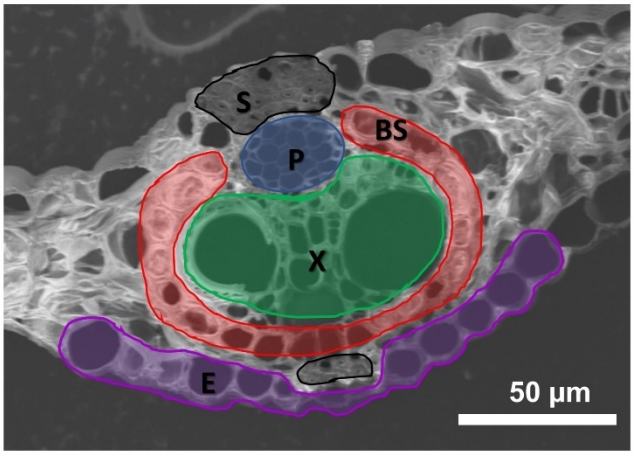

Figure 1. Scanning electron micrograph of a leaf section. Tissue types are coloured and marked: phloem (P) in blue, xylem (X) in green, bundle sheath (BS) in red, sclerenchyma (S) in black, and epidermis (E) in purple.

Locating and quantifying the different components of plant tissues has been a challenging and important research question, attracting attention across a broad range of fields, including plant molecular biology, agronomy, plant physiology and plant nutrition.[1,8] The visualization of plant tissues at the microscopic[7a,9] and nanoscopic scales[10,11] is a prerequisite to understanding their function, based on the development of their complex structures. Compositional insights, including molecular structure and interactions, may be gained by optical spectroscopy. Vibrational spectroscopies were successfully

[a] *Dr. V. M. R. Zancajo, Prof. Dr. R. Elbaum, Prof. Dr. J. Kneipp*
School of Analytical Sciences Adlershof (SALSA)
Humboldt-Universität zu Berlin
Albert-Einstein-Str. 5–9, 12489 Berlin (Germany)
E-mail: janina.kneipp@chemie.hu-berlin.de
[b] *Dr. V. M. R. Zancajo, Dr. S. Diehn, Prof. Dr. J. Kneipp*
Department of Chemistry
Humboldt-Universität zu Berlin
Brook-Taylor-Str. 2, 12489 Berlin (Germany)
[c] *Dr. V. M. R. Zancajo, Prof. Dr. J. Kneipp*
BAM Federal Institute for Materials Research and Testing
Richard-Willstätter-Str. 11, 12489 Berlin (Germany)
[d] *Prof. Dr. R. Elbaum*
R. H. Smith Institute of Plant Sciences and Genetics in Agriculture
The Hebrew University of Jerusalem
Rehovot 7610001 (Israel)

Supporting information for this article is available on the WWW under https://doi.org/10.1002/anse.202200006

coupled with a microscope in order to chemically characterize the micro-structures in plants, and were used to image distributions of lignin, cellulose, carbohydrates, proteins, and lipids, and to evaluate differences in plant organ composition.[12] Both Fourier-transform infrared (FTIR) and Raman microspectroscopy have been applied.[13] The sampling requirements, available diagnostic spectral bands, and spectral interferences in the plant samples, as well as spatial resolution differ considerably between both spectroscopies. Since they provide different spectral information due to different selection rules, it can be useful to combine both and use them together. In recent work, such a combination of FTIR and Raman spectroscopy was shown to provide a better understanding of the relationship between the mechanical properties and the lignin composition in poplars,[14] as well as of the cell wall composition of vascular tissues in Arabidopsis plants.[15] Similarly, the combination of Raman and FTIR with mass spectrometry allowed to evaluate subtle chemical variations in pollen chemistry.[16] Raman spectra of lignocellulosic plant materials exhibit strong autofluorescence[17] that is often aimed to be minimized.[9c,17a] Autofluorescence of cell walls has been observed at various wavelengths as a consequence of specific molecular structures and composition. Fluorescence microscopy allows high resolution imaging and the detection of cell wall components such suberin, lignin, proteins and chlorophyll.[18] Nevertheless the obtained chemical information is limited and therefore should be complemented with other types of spectroscopies such as Raman or FTIR.[19] The laser-induced autofluorescence of lignin is especially intense in Raman experiments at the excitation wavelength of 532 nm.[20] Therefore, it is possible to exploit the information contained in the Raman fluorescence background and combine it with the vibrational spectroscopic information.

The objective of this work is a comprehensive characterization of the organic and inorganic components of the plant tissue. We studied the composition of leaf cross sections extracted from sorghum plants grown with and without silicic acid supplementation. Special attention was paid to silicified structures, where we added information from autofluorescence microscopy and scanning electron microscopy coupled with energy-dispersive X-ray spectroscopy (SEM-EDX) to FTIR and Raman microspectroscopy datasets. The incorporation of the information contained in autofluorescence signals with vibrational spectroscopy led to a comprehensive characterization of molecular lignin structures. The results demonstrate that the combination of imaging modalities with sensitivity for organic and inorganic tissue components, respectively, and complementary spectroscopic information achieves a spatially resolved comprehensive characterization of the silicified plant tissue.

Results and Discussion

Multimodal imaging to evaluate the distribution of organic and inorganic components. The work was conducted on sections of leaf tissue from sorghum plants that were hydroponically grown and supplemented with silicate (+Si), and leaf tissue from non-supplemented plants (–Si). For the experiments, regions of the leaf veins were selected, and Raman and FTIR microspectra were collected to evaluate the chemical composition, structure, and interactions in the three basic leaf tissues. Figure 2 displays SEM images and FTIR and/or Raman spectroscopy chemical maps, of the same leaf sections. The FTIR maps provided a large overview over the different areas of the sections while the Raman mapping presented with micron precision and allowed to study the walls of individual cells.

The FTIR chemical maps (Figure 2E, F, J, K, O, P, T and U) were collected from de-paraffinized sections. They covered the whole vein here and provide a visualization of the relative abundance of important cell wall components across the section. The band at 1734 cm^{-1}, assigned to the C=O stretching vibration of lignin,[21,22] was used to visualize the distribution of lignin in the maps (Figure 2E and 2F). It shows particularly high signals in the xylem and the epidermis, in agreement with previous observations that were made in sections of Arabidopsis.[15] Many spectra contained a band at 1660 cm^{-1}, assigned to a contribution by the amide I mode[23] and a signal at 1520 cm^{-1} that could be ascribed to an amide II mode.[21,22,24] These two bands co-localize in the maps and enable mapping of the protein content (Figure 2J, K, O and P). They were particularly intense in spectra taken from the bundle sheath and chlorenchyma. Although the 1660 cm^{-1} band is generally assigned to the amide I mode, chlorophyll aldehydes or their degradation products may also contribute to it.[23] Polysaccharides and hemicelluloses were visualized using the band at 1037 cm^{-1} (Figure 2T and U) that is assigned to a C–O–C stretching mode[25] and show the highest intensity in the sclerenchyma.

Raman maps were collected from sections obtained from two types of preparation, the fixed samples cut for FTIR mapping (Figure 2G, L Q and V) and fresh samples (Figure 2H, I M, N, R,S,W and X) containing water. In the Raman data, the distribution of lignin could be mapped by plotting the intensity of the band at 1597 cm^{-1} assigned to C=C and C=O stretching vibrations of aromatic compounds and lignin.[26] The maps confirmed the FTIR results, that xylem tissues present a high content of lignin, contrasting with the relatively low amount detected in phloem tissue (Figure 2E, F, G and H). On the contrary, cellulose and hemicelluloses signals were particularly high in the phloem and sclerenchyma, also in good agreement with the maps obtained from the FTIR data. In the Raman data, the band at 1493 cm^{-1} can be assigned to C=C skeletal and C–N stretching vibrations of aromatic compounds and of proteins[27] as well as to calcium oxalate.[28] Strong contributions of this signal were observed in the cell walls of bundle sheath cells (Figure 2M and N). This simple chemical mapping using univariate analysis considers only one specific signal (which corresponds to a particular molecular group) at a time. The examples of co-localization of different vibrational modes of the same molecular group in the FTIR and Raman maps strongly supports our interpretations. Combining both types of spectra could be used to improve the mapping of molecules that show only a small number of strong signals in each of the spectroscopic approaches.

Research Article
doi.org/10.1002/anse.202200006

Chemistry Europe
European Chemical Societies Publishing

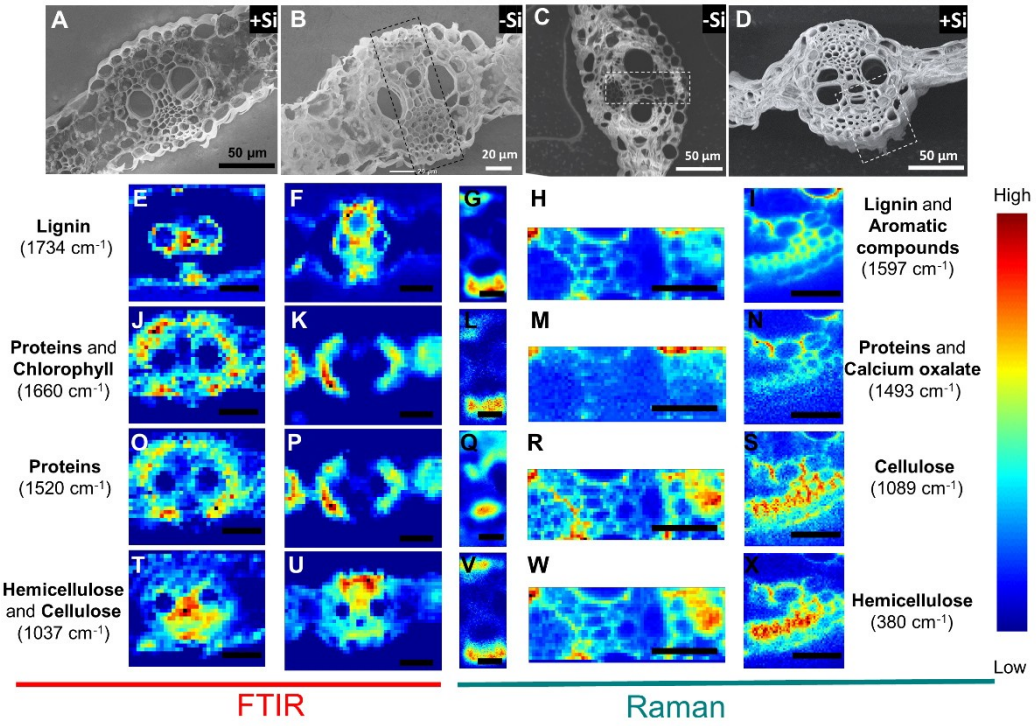

Figure 2. Scanning electron micrographs and chemical maps of sections obtained from leaf samples that were (A, B) fixed and embedded in paraffin, and (C, D) freshly cut. The sections were prepared from leaves of plants that were grown with silicic acid supplementation (marked in the upper right corner as + Si, A, D) and without silicic acid supplementation (-Si, B, C), respectively. Chemical maps were collected from both + Si and -Si, showing the distribution of lignin, proteins, chlorophyll, cellulose and hemicelluloses, based on the Raman peak intensity/absorbance at vibrational frequencies that are characteristic of the respective compounds as indicated. In this figure, -Si fixed sample, presented in (B), is used to demonstrate the chemical maps obtained from both, FTIR and Raman data are shown (F and G, K and L, P and Q, U and V, respectively). Scale bars: 40 µm for the FTIR maps (E, F, J, K, O, P, T, U) and 30 µm for the Raman maps (all other panels). All maps use the full min-max intensity scale.

To complement the vibrational information, SEM and light microscopy images of unstained samples were taken and compared to EDX and autofluorescence maps (Figure 3). The EDX maps show the distribution of silicon atoms, which are bound in cell walls as biogenic silica (Figure 3B).[7b] Interestingly, Si distribution (Figure 3B) correlates with lignin in the epidermis (Figure 2A), supporting a possible involvement of specific lignin structures in silica deposition that has been suggested on several occasions.[7a,29] However, a high amount of lignin was also detected in the xylem vessels where no silica deposition was found, suggesting that only specific lignin types may contribute to the silica deposition at specific locations.[30]

In the unfixed tissue, blue fluorescence indicates the presence of lignin, which is also visible in the green and red fluorescence images.[31] Regions of the phloem and some spots of the epidermis displayed strong blue autofluorescence (Figure 3C left image) attributed to the presence of suberin in the phloem and flavonoids in the epidermis..[18,31] The blue autofluorescence also diminished drastically after the preparation for FTIR analysis (Figure 3C right image).

Freshly cut, unfixed samples displayed a very strong red autofluorescence in the chlorenchyma and bundle sheath (Figure 3E), likely due to the presence of chlorophyll from chloroplasts.[9b] This fluorescence with a maximum at 680 nm has been reported as an undesired background signal that can hamper imaging experiments.[32] In contrast, the fixed samples prepared for FTIR analysis did not display such fluorescence. Instead, a low intensity signal was observed in the fibre cells of the sclerenchyma above and below the vascular bundle. The removal of the strong red fluorescence must be a consequence of the fixation, dehydration, paraffin embedding and de-paraffination process used here for practical reasons to work with water-free samples.

It is likely that the red-emitting fluorescent and highly reactive porphyrin structure of chlorophyll was degraded and washed in the chemical fixation.[33] In this regard, the location of signals from chlorophyll in the FTIR chemical maps discussed above (Figure 3J and 2 K) is consistent with the red fluorescence observed in bundle sheath (Figure 3E), suggesting the contribution of chlorophyll aldehydes.[18]

Vibrational spectra reflect the chemical differences between the tissue types. The vibrational and elemental maps as well as the fluorescence images clearly showed differences between three tissue types in the samples, i.e., epidermis, vasculature, and ground tissue (parenchyma and sclerenchyma). The Raman spectra were analysed in detail to discuss differences in composition and structure between these tissue types in the unfixed, hydrated samples. The spectra were sorted in groups using hierarchical cluster analysis (HCA) (Figure S2), and clusters containing only spectra of one of the tissues were selected and further analysed. Average Raman spectra of each of the tissues were very rich in bands (Figure 4A). All tentative assignments

Research Article
doi.org/10.1002/anse.202200006

Chemistry Europe
European Chemical Societies Publishing

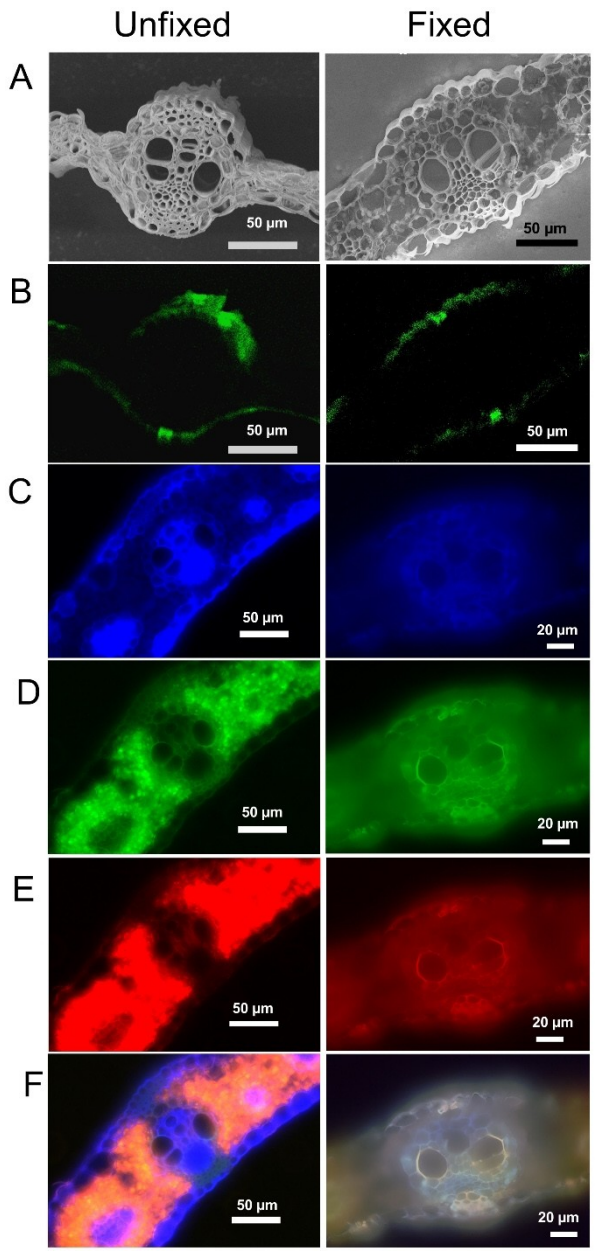

Figure 3. Multimodal imaging of an unfixed sample (left column) and a fixed sample (right column). (A) SEM micrographs, (B) EDX maps showing the distribution of silica in green, (C–F) autofluorescence images (C) in the blue, (D) in the green, and (E) in the red, as well as (F) and their composite image. Note that some cells in the bundle sheath and the mesophyll collapsed during SEM imaging of the unfixed sample (left column). The two samples are those shown in Figure 2D and 2 A, respectively.

to vibrations and the different cell wall components are summarized in Table S1 of the Supporting Information. The spectra were dominated by the C=C and C=O stretching vibrations of lignin,[34] causing bands between 1550 cm^{-1} and 1660 cm^{-1} with a pronounced maximum at 1597 cm^{-1}. Depending on the tissue, this band displays a shoulder or an individual band around 1570 cm^{-1}. The 1570 cm^{-1} band has been reported in dry wood, where it was ascribed to lignin radicals that are intermediates in lignin biosynthesis.[35] Several bands that are also clearly assigned to lignin can be observed in the spectra. The band at 1624 cm^{-1} arises from the C=C stretch of coniferyl (guaiacyl, G) aldehyde.[26b] The band at 1331 cm^{-1}, an aliphatic O–H bending mode, is especially prominent in spectra from the bundle sheath (Figure 4A, red trace) and indicates the presence of sinapyl (S) units in lignin.[36] The band at 1373 cm^{-1} is assigned to both lignin G and S units,[37] and was more intense in xylem and phloem spectra (Figure 4A, green and blue traces) than in the other tissues. The characteristic C–C and C–O stretching vibrations of cellulose[34,38] appear as a doublet at 1089 cm^{-1} and 1115 cm^{-1} in the Raman spectra of the sorghum leaf (Figure 4A). They were also of particularly high intensity in the spectra taken from xylem and phloem (Figure 4A). The band at 890 cm^{-1} that is found in all the tissues corresponds to skeletal deformation and side chain vibrations of cellulose and hemicelluloses.[36b] Hemicellulose together with other polysaccharides causes several additional Raman bands in the low frequency range, including C–O–C, H–C–C, H–C–O, H–O–C, and C–C–C deformation vibrations at 520 cm^{-1}, 498 cm^{-1}, 428 cm^{-1} and 370 cm^{-1}.[26d,36] These bands overlap with the Si–O–Si bending vibration, which would be expected as a broad and very low intensity band.[39] Therefore, silica is not distinguishable in the Raman spectra, in spite of its clear presence in the region of the epidermis, as seen by EDX mapping (Figure 3B). Other silica related vibrations, including the Si–O–Si symmetric stretching around 800 cm^{-1}[39] and the Si–OH stretching at 975 cm^{-1}, were not observed due to overlap with the C–C, C–O, and C–O–C stretching and the C–C–H deformation modes of cellulose and hemicelluloses.[37a]

The epidermis spectra (Figure 4A, purple spectrum) showed intense bands that we attribute to the presence of waxes and aliphatic compounds in the cuticle, including the CH_2 bending mode at 1456 cm^{-1}, and other deformation modes of CH_2 and CH_3 groups around 1420 cm^{-1}, and of C–C–H groups at 1260 cm^{-1}.[40] The bands at 1197 cm^{-1} and 1493 cm^{-1} were observed in spectra taken from the bundle sheath and in some spectra of sclerenchyma (Figure 4A, red and black trace). The former could be assigned to a C–H bending mode and the latter to calcium oxalate[28] and a C–N stretching vibration coupled with vibrations of amino radical cations and C=C skeletal vibrations of aromatic compounds.[27]

Interestingly, the Raman spectra from all tissues except from the bundle sheath showed a small band at 1524 cm^{-1}, assigned to the pronounced C=C stretching mode in the spectrum of carotenoids.[41] Its low intensity observed here, in contrast with the reported high intensity in other studies, is most probably a consequence of the long excitation times with a wavelength in pre-resonance that result in quick photobleaching, decreasing the contribution of carotenoids in the spectra.[12c,41] The complexity and variability of these thousands of spectra require the use of multivariate analysis tools to evaluate the chemical differences between the tissues. The spectroscopic data were further analysed by HCA and principal component analysis (PCA), which are very efficient for evaluating such large spectroscopic data sets.[26d,42] PCA provides an easy means of exploratory data analysis, as it is a non-parametric method able to reduce and extract relevant

Research Article
doi.org/10.1002/anse.202200006
Chemistry Europe
European Chemical Societies Publishing

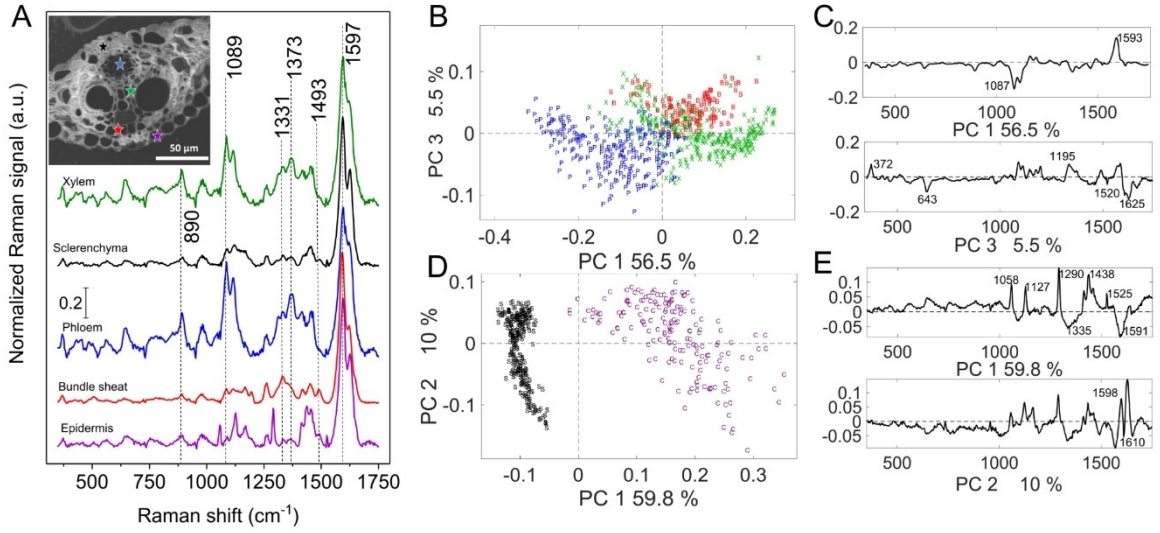

Figure 4. (A) Raman spectra of the epidermis (average of 176 spectra) in purple, bundle sheath (average of 126 spectra) in red, phloem (average of 244 spectra) in blue, sclerenchyma (average of 272 spectra) in black and xylem (average of 288 spectra) in green of sorghum leaves obtained after classification using HCA. For orientation, some bands are labelled. Results of the PCA of selected spectra from different tissues. (B, C, D and E). PCA scores plot of spectra taken from vascular tissue (B), separation according to the tissue (xylem- X, green, phloem- P, blue and bundle sheath- B, red) was achieved. (C) PC1 and PC3 loadings indicating bands responsible for the separation. (D) A clear separation was achieved for spectra from epidermis and sclerenchyma in the score plot along PC1, which contains 58,9 % of the variance in a data set consisting of 448 spectra. (E) The chemical differences between these tissues can be further understood by examination of the loadings and direct comparison with spectra.

information from the spectral data.[43] HCA was used to classify spectra according to the tissue type (Supporting Figure S2) and then was combined with PCA. Rather than submitting all spectra to one single classification analysis, here, a sequential approach was used, where first, spectra from epidermis and sclerenchyma tissue and those from the vascular tissue, respectively, were extracted from the mapping data sets, that were then compared further.

The analysis of Raman spectra taken from vascular tissue showed that it is possible to discriminate between spectra from phloem, xylem, and bundle sheath (Figure 4C). The observation of differences in the chemical composition of phloem versus xylem was also reported for Arabidopsis.[15] The spectra assigned to the xylem showed the highest intra-class variation. The separation of phloem and xylem spectra along PC1 was largely caused by a high influence of the bands assigned to cellulose, suggesting a higher contribution of it in phloem cells in comparison with the other tissues (Figure 4D). PC1 also showed a high influence of the band at 1593 cm^{-1} assigned to lignin. This indicates differences between the tissues in lignin composition. PC3 that separated the phloem and xylem from the bundle sheath spectra was influenced by the bands at 1335 cm^{-1} and at 372 cm^{-1} and the bands at 1625 cm^{-1} and 643 cm^{-1} (Figure C). This band combination is assigned to sinapyl units, thus supporting a higher proportion of S lignin units in the bundle sheath than in phloem and xylem (Figure 4B and C, bottom). The band at 1493 cm^{-1} also contributed to the separation, being more intense in the bundle sheath than in the other tissues.

Figure 4D shows the results of the PCA of spectra taken from the sclerenchyma and outer part of the epidermis. (cf. Figure 1). The PCA scores plot showed a clear separation between these tissues along the first principal component. The loading of PC1 (Figure 4E) indicated that the separation is based on bands that are assigned to aliphatic compounds and lipids at 1058 cm^{-1}, 1127 cm^{-1}, 1290 cm^{-1} and 1438 cm^{-1} and the band assigned to carotenoids at 1525 cm^{-1}. The associated chemical groups were more abundant in the epidermis outer cell wall than in the sclerenchyma. The separation is also caused by variation in lignin composition as indicated by the signals at 1335 cm^{-1} and 1591 cm^{-1} in the loadings plot (Figure 4E). The loading of PC2 did not contribute to the separation according to the tissue types but rather shows a dispersion of the data within each tissue. This suggested variation in the lignin structure and composition within the tissues, as evidenced by the bands assigned to lignin that influence the loadings, (see Figure 4C, bottom). Lignin was detected by its Raman signals in the xylem and sclerenchyma (Figure 4A, black and green trace) specifically by the pronounced band at 1370 cm^{-1}, assigned to deformation modes of CH_3 and CH_2 groups, which appeared together with the lignin-specific band at 1235 cm^{-1}.[21]

The FTIR spectra are equally rich in bands as their Raman counterparts, but the signals appear broader and more overlapping (Figure 5). The most intense bands are summarized in Supporting Information Table S2, together with their tentative assignments to vibrations and the different cell wall components. The wavenumbers and their assignments presented here are shifted with respect to those of isolated polymer compounds reported in previous work. This may be due to the different chemical environments of the spectroscopically active groups and the wide unresolved bands of heterogeneous and interacting polymeric structures. The strongest bands in the FTIR spectra of all tissues arise from the C–O–C stretching

Research Article
doi.org/10.1002/anse.202200006

Chemistry Europe
European Chemical Societies Publishing

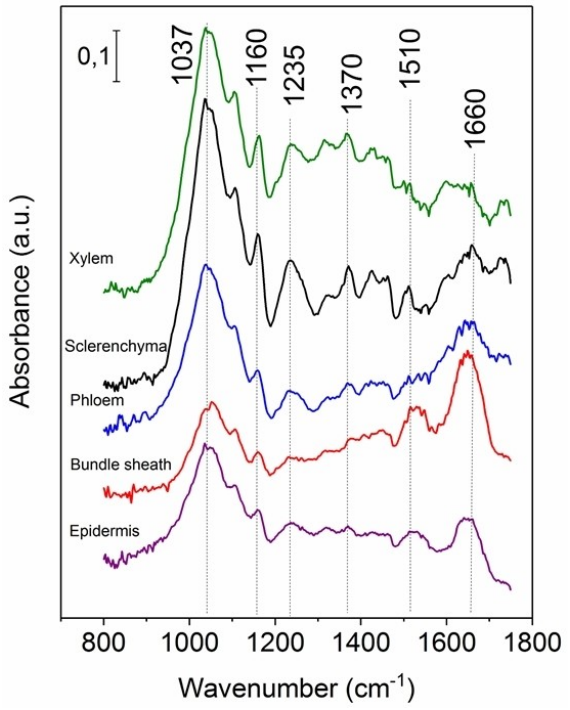

Figure 5. Representative FTIR spectra of the epidermis, bundle sheath, phloem, sclerenchyma and xylem of sorghum leaves. For orientation, some vibrations are labelled.

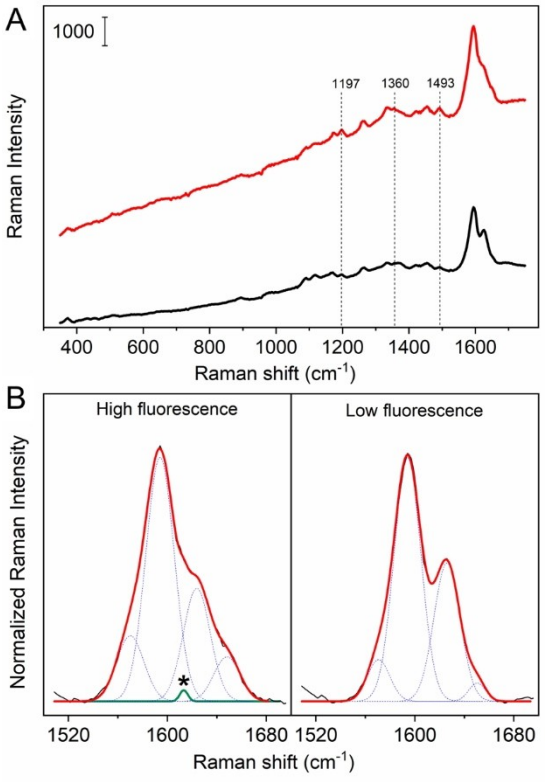

Figure 6. (A) Averages of the spectra in clusters containing 87 spectra with high fluorescence contribution (red) and 116 spectra with low fluorescence (black) from sclerenchyma tissue. To visualize the background in the red spectrum, the traces are not offset. (B) Deconvolution of the Raman bands in the range from 1500 to 1750 $cm^{-1}$for the high and low fluorescence average spectra after baseline correction. The asterisk marks the component with the maximum at 1613 cm^{-1} required only for the fitting of high fluorescence spectra.

vibrations of carbohydrates such as cellulose and hemicelluloses[25] e.g., at 1037 cm^{-1}. Spectra from bundle sheath and epidermis showed in addition a pronounced component at 1051 cm^{-1}, suggesting a variation in the composition of the polysaccharides. Similar to the Raman spectra, the bands of silica were not observed in the FTIR microspectra of the sorghum samples. The Si–O stretching mode, expected around 1100 cm^{-1} for silica containing cell walls such as the epidermis (cf. Figure 2B) was masked by the other spectral features. This is in contrast to localized nano-IR measurements, where the masking/averaging effect is not present, and even small, pure phytolith structures can be found.[7c] Absorptions at 1660 cm^{-1}, 1520 cm^{-1}, and 1315 cm^{-1}, are assigned to proteins, representing amide I, amide II, and amide III bands, respectively,[24a] and to chlorophyll and lignin.[21] Separation of the contributions of these polymers solely based on the FTIR maps is rather challenging.

Lignin bond types and structure from combined autofluorescence and Raman spectra. Most of the Raman spectra showed a strong fluorescence induced by the Raman excitation laser. We investigated its cause using multivariate analysis and a deconvolution of the Raman signals. HCA of the raw spectra obtained from the sclerenchyma tissue led to a classification that is based on the overall intensity of the Raman signal, greatly influenced by changes in the background autofluorescence. Three clusters formed, containing spectra with high, medium and low or no fluorescence background (data not shown). The average spectra of the groups presenting high and low-to-non-fluorescence are displayed in Figure 6A. PCA effectively separated the two spectral groups (Supporting Figure S3A). The spectra with strong fluorescence contribution showed higher intensity of the Raman signals assigned to lignin moieties (marked in Supporting Table S1), as indicated by the PCA loadings (Supporting Figure S3B). In contrast, in the spectra with no fluorescence contribution a higher relative contribution of the bands associated with cellulose, and, interestingly, to bands associated with G units in lignin was found. The band at 1493 cm^{-1} of aromatic compounds, proteins,[27] and/or calcium oxalate[28] also influences the separation.

Differences in the lignin band in the range 1500 cm^{-1} to 1750 cm^{-1}[44] were found between the average spectra of the high fluorescence and low-to-non-fluorescence spectral groups. The 1550–1750 cm^{-1} region is the most characteristic and informative region of the Raman spectrum of lignin contributions, with aromatic rings, ethylenic C=C bonds, and α- and γ-C=O functional groups contributing their vibrational modes.[34] Deconvolution analysis of this region showed that the fitting of the high fluorescence spectrum only converged when a band at 1613 cm^{-1} was considered (Table 1). In contrast, in the low fluorescence spectra, this band had to be excluded for the

Research Article
doi.org/10.1002/anse.202200006
Chemistry Europe
European Chemical Societies Publishing

Table 1. Parameters of the best fit obtained for the 1500 to 1750 cm^{-1} spectral range of the average spectra of sclerenchyma with high fluorescence background and low fluorescence background (cf. Figure 6A).

High fluorescence Raman shift [cm^{-1}]	Area [%]	Peak shape	Low fluorescence Raman shift [cm^{-1}]	Area [%]	Peak shape
1570	13.8	Gaussian	1570	8.2	Gaussian
1594	53.2	Gaussian	1594	57.3	Gaussian
1613	0.7	Gaussian	1613	Absent	
1624	23.4	Gaussian	1624	31.7	Gaussian
1648	8.9	Gaussian	1648	2.7	Gaussian

model to converge (Figure 6B). The contributions of the different components are listed in Table 1.

The band at 1613 cm^{-1}, unique to the sclerenchyma samples with high fluorescence, has been assigned to biphenyl out-of-phase ring vibrations in dibenzodioxocin.[45] Biphenolic structures show in addition bands at 1197 cm^{-1} and 1360 cm^{-1}[45] that were also more intense in the high fluorescence spectra as compared to low fluorescence spectra (Figure 6A).

It should be noted that the conjugation of C=O double bonds to aromatic rings increases their Raman scattering signals, and the presence of conjugated structures and pre-resonance effects in lignin can have implications to band intensities.[44] Nevertheless, the observation made here confirms a previous attempt to clarify potential correlations between the laser-induced fluorescence and lignin structure by Raman spectroscopy in lignin model compounds.[20] There, Lähdetie and co-workers concluded that the presence of free phenolic structures was not a prerequisite for the fluorescence. Instead, the bond types, especially the 5–5′ structures via the conjugation system over the two aromatic rings strongly influence the fluorescence of lignin model compounds.[20] Furthermore, flexible conformations display higher intensities of fluorescence than structurally rigid models.[20] In this work, we observed this effect in situ in the native tissue. A schematic of lignin formation, showing the different conformations and bond types is displayed in Figure 7. In summary, our data strongly suggest that the lignin conformation, specifically the 5–5′ linkages that produce biphenyl structures are the most influencing factor of the lignin fluorescence properties in the plant cell wall. The co-localization of specific Raman spectra and fluorescence properties with silicification patterns here suggests that both spectroscopies could be used to study the role of lignin in biosilicification.

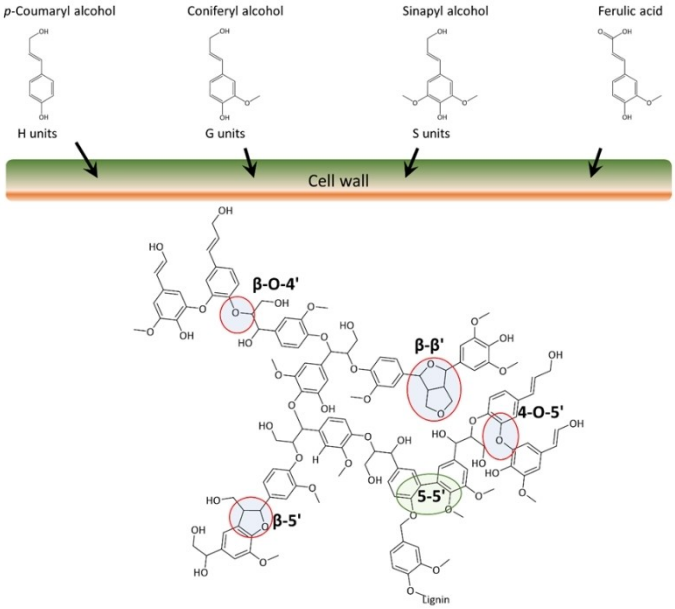

Figure 7. Scheme summarizing lignin formation as proposed in previous work[46] and indicating the structures that lead to fluorescence. Canonical grass monolignols are incorporated into the polymer through different types of bonds marked in the lignin structure by red circles. The 5′-5′ bond forming the biphenyl structure is surrounded by a green circle.

Conclusion

In this work, we aimed to better understand the plant cell wall organic matrix, in which silica is deposited. Leaf cross-sections of sorghum plants grown with and without supplementation of silicic acid were analysed by microscopy and spectroscopy. A multimodal approach, comprising vibrational microspectroscopy, fluorescence microscopy, and electron microscopy combined with elemental probing by SEM-EDX was applied. The distinction between plant cell wall components is challenging, specifically regarding a discrimination of cellulose from other cell wall polymers, and the complexity of lignin as extremely heterogeneous macromolecular structure. Raman and FTIR spectra from different tissue regions were extracted from the data sets and compared by multivariate methods.

The combination of Raman and infrared microspectroscopy, each yielding chemical maps at different microscopic resolution, indicated a specific composition of the different tissue types regarding the abundance of the several macromolecular tissue components. Lignin structure was variable and specific of the different tissue types. Xylem and phloem showed relative higher amounts of cellulose than the rest of the tissues. Proteins, chlorophyll and calcium oxalate were abundant in the bundle sheath, whereas the epidermis was rich in waxes and suberin.

While all the approaches evaluated here are useful to image the plant structures and illustrate plant tissue complexity at different length scales, a connection of different molecular properties was aimed for by comparing spectral information. In the tissue cross sections, SEM enabled an assignment of focal volumes/locations to particular cells/cell walls in the sections. In particular, SEM-EDX mapping connected locations in the

Raman maps to regions with high silicon content. Nonetheless, the contribution of the silica itself to the vibrational spectra was masked by contributions from the organic matrix. The combination of the two complementary vibrational micro-spectroscopies with SEM-EDX provides an extremely suitable and comprehensive method to get structural information from mineralized plant tissues.

The comparison with the FTIR spectral mapping information enabled the conclusion that part of the autofluorescence in the region of the bundle sheaths must be due to the presence of chlorophyll degradation products. The use of different preparation methods, in order to optimize the samples for the water-free mapping by FTIR microscopy clearly indicated that a correlation of vibrational and fluorescence information is optimal when native, hydrated tissue sections are used. The origin of autofluorescence of the tissue was analysed in more detail, as it was a major hallmark of many Raman spectra that were excited with a wavelength of 532 nm. Multivariate analysis revealed different fluorescence contributions within different regions of sclerenchyma tissue. Detailed qualitative analysis of the pre-resonant Raman signals of lignin enabled a correlation of the molecular structure of lignin and its fluorescence properties. Our results support the presence of flexible lignin conformations at locations of higher intensities of fluorescence in situ in the native tissue for the first time, in agreement with previous work on synthetic lignin models.

In the future, the combination of the vibrational and elemental information in one type of hyper-spectral image is desirable and being developed, similar to a recently presented approach that demonstrated the hyperspectral images of FTIR and Raman information.[47] The role of lignin and other cell wall components in the biomineralization in other plant tissues should be further studied, as substantial variation in cell wall autofluorescence is found between silica deposition sites and the rest of cell walls, such as sorghum roots, where autofluorescence depends on silicon supplementation/deprivation.[29b] The future in situ structural characterization of the lignin in such tissue regions will help to further delineate the relationship between the lignin structure and molecular composition and silica deposition without the need to isolate the lignin and to disrupt its interaction with the other cell wall components.

Experimental Section

Plant material and growing conditions

Grains of similar morphology from *Sorghum bicolor* (L.) Moench (wild type; line BTx623) were selected and germinated in the dark, at ambient temperature and wrapped in wet paper. Seedlings were either grown in hydroponic media containing only Hoagland nutrient solution (0.5 mM KNO_3, 0.15 mM $Ca(NO_3)_2 \cdot 4H_2O$, 0.1 mM $NH_4H_2PO_4$, 0.1 mM $MgSO_4 \cdot 7H_2O$, 0.03 μM $CuSO_4 \cdot H2O$, 0.06 μM $Na_2MoO_4 \cdot 2H_2O$, 0.16 μM $ZnSO_4 \cdot 7H_2O$, 0.91 μM $MnCl_2 \cdot 4H_2O$, 4.63 μM H_3BO_3, 2 μM EDFS ($C_{10}H_{12}N_2NaFeO_8$) in Milli-Q (Millipore) water), in case of treatment without the addition of silica, or Hoagland solution containing sodium silicate ($NaSiO_4$) at a final concentration of 2 mmol/L. The plants were grown indoor under artificial light (18hours/day) at the Chemistry department of Humboldt-Universität zu Berlin. The hydroponic solutions were changed regularly every 3–4 days, and the pH was adjusted to 5.8. Aeration to the roots was provided by an air pump (200 l/hour). Up to 4 plants were grown in the same 2 litre pot for up to 185 days.

Raman and FTIR spectroscopy

Raman maps were collected from cross-sections of sorghum leaves that were manually cut and placed between two CaF_2 windows with a drop of water to prevent photodamage and to decrease autofluorescence. The disks were sealed with paraffin to prevent water evaporation. Raman maps were acquired with a Horiba LabRam HR microspectrometer (Horiba Jobin Yvon, Bensheim, Germany) using a 532 nm laser with a power of 8.5 mW as excitation source that was focussed into a spot of 1.3 μm nominal diameter, corresponding to an intensity of $\sim 1.6 \times 10^5$ W/cm^2. Spectra were recorded using a 300 lines/mm grating and a liquid nitrogen cooled CCD detector. Spectra were acquired by raster-scanning with a step size of 1 μm in x- and y-direction, with an acquisition time of 2 s and 22 accumulations per spectrum in the spectral range from 200 to 4000 cm^{-1}. A total of 12 maps of Si-supplemented samples and 5 maps of Si starved plants were obtained.

For the FTIR maps, samples were collected from sorghum leaves, cut into pieces, fixed with a mixture of formaldehyde, ethanol, and acetic acid (FAA), 10%:50%:5% + 35% water, dehydrated with an ethanol series (50, 60, 70, 80, 90 and 100% ethanol, 100% isopropanol), and embedded in paraffin. The paraffin blocks were cut to sections of 20 μm thickness, which were mounted in zinc selenide windows and de-paraffinized with hexane.

IR transmission spectra were collected using an FTIR microscope (ThermoNicolet) using the synchrotron light source at the IRIS beamline of BESSY-HZB, Berlin, Germany. The size of the microscope aperture, determining the spot size from which the spectrum is acquired, was set to 12 μm × 12 μm. Spectra were obtained at a spectral resolution of 1.93 cm^{-1} in the range 700–4000 cm^{-1} by averaging 64 interferograms. The step size varied depending on the sample between 3 μm and 5 μm. A total of 9 maps of Si supplemented plants and 9 maps of Si starved plants were recorded.

The spectra were pre-processed for further analysis using MatLab (The MathWorks, Inc., Ismaning, Germany) and CytoSpec (CytoSpec, Inc., Berlin, Germany) software. Data pre-processing included the elimination of spikes, interpolation, baseline correction using asymmetric least squares (AsLS),[48] vector-normalization, and calculation of derivatives. For chemical mapping, intensities of individual bands were determined from the original spectra after baseline correction. Hierarchical cluster analysis (HCA) was carried out with raw spectra, baseline corrected spectra, vector-normalized spectra and first and second derivatives using the spectral range 360–1750 cm^{-1}. Principal component analysis (PCA) was carried out with pre-processed spectra using the spectral range 360–1750 cm^{-1}.

Scanning Electron Microscopy-Energy-dispersive X-ray spectroscopy (SEM-EDX)

Leaves were dissected mechanically in segments, and epidermis sections and cross-sections were prepared manually using a razor blade. The sections were either supported on carbon tape or on ZnSe windows as used for FTIR spectroscopic analysis. The sections were analysed with a JCM-6000PLUS NeoScope scanning electron microscope (JEOL, Japan) using an accelerating voltage 15 kV in the low vacuum mode. The silicon elemental maps of the observed

samples were obtained with the same instrument by energy-dispersive X-ray analysis. Si elemental maps were obtained by EDX with a dwell time of 2 ms, high probe current, and gain set to 1.

Fluorescence imaging

Autofluorescence microscopy images were obtained after mounting the samples in calcium fluoride windows for the Raman maps or zinc selenide windows for the FTIR maps with a light microscope BX23, (Olympus, Hamburg, Germany) with a 20x objective. The red autofluorescence images were recorded with excitation with a wavelength in the range 530–550 nm and a cut off filter at 575 nm. The blue autofluorescence images were recorded with excitation with a wavelength in the range 330–385 nm and a cut off filter at 420 nm. The green autofluorescence images were recorded with excitation with a wavelength in the range 460–495 nm and a cut off filter at 510 nm. All images were taken using CellSens Standard Software 1.17 (Olympus, Hamburg, Germany).

Acknowledgements

We thank HZB-BESSY for the allocation of beamtime and Dr. Ljiljana Puskar for support at the IRIS beamline. The work was supported by funding for the School of Analytical Sciences Adlershof by Deutsche Forschungsgemeinschaft (DFG GSC1013 SALSA). V.M.R.Z. acknowledges support by a fellowship from DFG GSC 1013 SALSA. Open Access funding enabled and organized by Projekt DEAL.

Conflict of Interest

The authors declare no conflict of interest.

Data Availability Statement

The data that support the findings of this study are available from the corresponding author upon reasonable request.

Keywords: cell walls · lignin · multimodal imaging · silica · spectroscopy

[1] H. Hofte, A. Voxeur, *Curr. Biol.* **2017**, *27*, R865–R870.
[2] K. Sato, N. Ozaki, K. Nakanishi, Y. Sugahara, Y. Oaki, C. Salinas, S. Herrera, D. Kisailus, H. Imai, *RSC Adv.* **2017**, *7*, 13065–13071.
[3] L. Yongchao, N. Miroslav, B. Richard, G. Haijun, S. Alin, *Silicon in Agriculture. From Theory to Practice*, Springer, Netherlands, **2015**.
[4] M. Wang, L. Gao, S. Dong, Y. Sun, Q. Shen, S. Guo, *Front. Plant Sci.* **2017**, *8, 701*.
[5] D. Coskun, R. Deshmukh, H. Sonah, J. G. Menzies, O. Reynolds, J. F. Ma, H. J. Kronzucker, R. R. Belanger, *New Phytol.* **2018**, *129*, 67–85.
[6] S. Kumar, M. Soukup, R. Elbaum, *Front. Plant Sci.* **2017**, *8*, 438.
[7] a) M. Soukup, V. M. Rodriguez Zancajo, J. Kneipp, R. Elbaum, *J. Exp. Bot.* **2020**, *71*, 6807–6817;b) V. M. R. Zancajo, S. Diehn, N. Filiba, G. Goobes, J. Kneipp, R. Elbaum, *Front. Plant Sci.* **2019**, *10*, 1571; c) V. M. R. Zancajo, T. Lindtner, M. Eisele, A. J. Huber, R. Elbaum, J. Kneipp, *Anal. Chem.* **2020**.
[8] a) W. D. Wilson, J. M. Barwick, J. A. Lomax, M. C. Jarvis, H. J. Duncan, *Plant Sci.* **1988**, *57*, 83–90; b) S. Vorwerk, S. Somerville, C. Somerville, *Trends Plant Sci.* **2004**, *9*, 203–209; c) F. A. Pettolino, C. Walsh, G. B. Fincher, A. Bacic, *Nat. Protoc.* **2012**, *7*, 1590–1607; d) B. Zhang, Y. Gao, L. Zhang, Y. Zhou, *J. Integr. Plant Biol.* **2021**, *63*, 251–272; e) A. Heredia, A. Jiménez, R. Guillén, *Z. Lebensm.-Unters. Forsch.* **1995**, *200*, 24–31.
[9] a) M. Soukup, M. Martinka, M. Cigáň, F. Ravaszová, A. Lux, *Planta* **2014**, *240*, 1365–1372; b) H. K. Lichtenthaler, J. Schweiger, *J. Plant Physiol.* **1998**, *152*, 272–282; c) B. Bokor, M. Soukup, M. Vaculík, P. Vd'ačný, M. Weidinger, I. Lichtscheidl, S. Vávrová, K. Šoltys, H. Sonah, R. Deshmukh, R. R. Bélanger, P. J. White, H. A. El-Serehy, A. Lux, *Front. Plant Sci.* **2019**, *10*, 988 ; d) M. Soukup, M. Martinka, D. Bosnic, M. Caplovicova, R. Elbaum, A. Lux, *Ann. Bot.* **2017**, 120, 5, 739–753.
[10] V. V. Volkov, G. J. Hickman, A. Sola-Rabada, C. C. Perry, *Front. Plant Sci.* **2019**, 10, 210 .
[11] C. C. Perry, R. J. P. Williams, S. C. Fry, *J. Plant Physiol.* **1987**, *126*, 437–448.
[12] a) I. Liedtke, S. Diehn, Z. Heiner, S. Seifert, S. Obenaus, C. Büttner, J. Kneipp, *Spectrochim. Acta Part A* **2021**, *251*, 119418; b) N. Gierlinger, L. Goswami, M. Schmidt, I. Burgert, C. Coutand, T. Rogge, M. Schwanninger, *Biomacromolecules* **2008**, *9*, 2194–2201; c) I. Zeise, Z. Heiner, S. Holz, M. Joester, C. Buttner, J. Kneipp, *Plants* **2018**, *7*, 7.
[13] a) N. Gierlinger, M. Schwanninger, *Spectroscopy* **2007**, *21*; b) A. K. Hartwig Schulz, A. Naumann, G. Gudi, in: *Infrared and Raman Spectroscopic Imaging* (Ed.: W.-V. V. G. C. KGaA.), **2014**, pp. 225–294.
[14] a) M. Özparpucu, M. Rüggeberg, N. Gierlinger, I. Cesarino, R. Vanholme, W. Boerjan, I. Burgert, *Plant J.* **2017**, *91*, 480–490; b) M. Özparpucu, N. Gierlinger, I. Burgert, R. Van Acker, R. Vanholme, W. Boerjan, G. Pilate, A. Déjardin, M. Rüggeberg, *Planta* **2018**, *247*, 887–897.
[15] S. Dinant, N. Wolff, F. De Marco, F. Vilaine, L. Gissot, E. Aubry, C. Sandt, C. Bellini, R. Le Hir, *J. Exp. Bot.* **2018**, *70*, 871–884.
[16] S. Diehn, B. Zimmermann, V. Tafintseva, S. Seifert, M. Bağcıoğlu, M. Ohlson, S. Weidner, S. Fjellheim, A. Kohler, J. Kneipp, *Front. Plant Sci.* **2020**, *10*.
[17] a) R. H. Atalla, U. Agarwal, in *Microbeam Analysis*, **1984**; b) J. A. Olmstead, D. G. Gray, *J. Pulp Pap. Sci.* **1997**, *23*, J571–J581; c) D. Djikanović, A. Kalauzi, K. Radotić, C. Lapierre, M. Jeremić, *Russ. J. Phys. Chem. A* **2007**, *81*, 1425–1428.
[18] L. Donaldson, N. Williams, *Plants* **2018**, *7*, 10.
[19] Y. Mottiar, N. Gierlinger, D. Jeremic, E. R. Master, S. D. Mansfield, *New Phytol.* **2020**, *226*, 704–713.
[20] A. Lähdetie, P. Nousiainen, J. Sipilä, T. Tamminen, A.-S. Jääskeläinen, *Holzforschung* **2013**, *67*, 531.
[21] O. Faix, *Holzforschung* **1991**, *45*, 21.
[22] C. Sene, M. C. McCann, R. H. Wilson, R. Grinter, *Plant Physiol.* **1994**, *106*, 1623–1631.
[23] K. Ballschmiter, J. Katz, *J. Am. Chem. Soc.* **1969**, *91*, 2661–2677.
[24] a) J. Bandekar, *Biochim. Biophys. Acta Protein Struct. Mol. Enzymol.* **1992**, *1120*, 123–143; b) M.-A. Ha, I. M. MacKinnon, A. Šturcová, D. C. Apperley, M. C. McCann, S. R. Turner, M. C. Jarvis, *Phytochemistry* **2002**, *61*, 7–14.
[25] a) P. Robert, M. Marquis, C. Barron, F. Guillon, L. Saulnier, *J. Agric. Food Chem.* **2005**, *53*, 7014–7018; b) M. Kačuráková, P. Capek, V. Sasinková, N. Wellner, A. Ebringerová, *Carbohydr. Polym.* **2000**, *43*, 195–203.
[26] a) M. Makarem, C. M. Lee, K. Kafle, S. Huang, I. Chae, H. Yang, J. D. Kubicki, S. H. Kim, *Cellulose* **2019**, *26*, 35–79; b) P. Bock, N. Gierlinger, *J. Raman Spectrosc.* **2019**, *50*; c) J. S. Lupoi, S. Singh, R. Parthasarathi, B. A. Simmons, R. J. Henry, *Renewable Sustainable Energy Rev.* **2015**, *49*, 871–906; d) J. Lupoi, S. Singh, M. Davis, D. Lee, M. Shepherd, B. Simmons, R. Henry, *Biotechnol. Biofuels* **2014**, *7*, 93.
[27] F. S. Parker, *Applications of infrared*, *Raman and Resonance Raman spectroscopy in biochemistry*, New York, **1984**.
[28] N. Sasani, P. Bock, M. Felhofer, N. Gierlinger, *Plant Methods* **2021**, *17*, 17.
[29] a) U. Agarwal, S. A. Ralph, R. H. Atalla, in *ISWPC*, **1997**; b) N. Zexer, R. Elbaum, *J. Exp. Bot.* **2020**, 71, 6818–6829; c) C. Zhang, L. Wang, W. Zhang, F. Zhang, *Plant Soil* **2013**, *372*, 137–149; d) N. George, A. Antony, T. Ramachandran, F. Hamed, A. Kamal-Eldin, *Front. Plant Sci.* **2020**, *11*, 917.
[30] N. Zexer, R. Elbaum, *J. Exp. Bot.* **2021**, *73*, 1450–1463.
[31] L. Donaldson, *Molecules* **2020**, *25*, 2393.
[32] a) G. H. Krause, E. Weis, *Annu. Rev. Plant Physiol. Plant Mol. Biol.* **1991**, *42*, 313–349; b) Y. Kodama, *PLoS One* **2016**, *11*, e0152484.
[33] A. Hosikian, S. Lim, R. Halim, M. K. Danquah, *Int. J. Chem. Eng.* **2010**, *2010*, 391632.
[34] U. P. Agarwal, R. S. Reiner, S. A. Ralph, *Cellulose* **2010**, *17*, 721–733.
[35] S. Barsberg, P. Matousek, M. Towrie, H. Jørgensen, C. Felby, *Biophys. J.* **2006**, *90*, 2978–2986.
[36] a) U. P. Agarwal, *Molecules* **2019**, *24*, 1659; b) L. Sun, B. A. Simmons, S. Singh, *Biotechnol. Bioeng.* **2011**, *108*, 286–295.

[37] a) U. P. Agarwal, J. D. McSweeny, S. A. Ralph, *J. Wood Chem. Technol.* **2011**, *31*, 324–344; b) A.-M. Saariaho, A.-S. Jääskeläinen, M. Nuopponen, T. Vuorinen, *Appl. Spectrosc.* **2003**, *57*, 58–66.
[38] a) U. P. Agarwal, S. A. Ralph, R. S. Reiner, C. Baez, *Carbohydr. Polym.* **2018**, *190*, 262–270; b) N. Gierlinger, M. Schwanninger, A. Reinecke, I. Burgert, *Biomacromolecules* **2006**, *7*, 2077–2081.
[39] S. K. Sharma, J. F. Mammone, M. F. Nicol, *Nature* **1981**, *292*, 140–141.
[40] M. M. L. Yu, H. G. Schulze, R. Jetter, M. W. Blades, R. F. B. Turner, *Appl. Spectrosc.* **2007**, *61*, 32–37.
[41] F. Schulte, J. Mader, L. W. Kroh, U. Panne, J. Kneipp, *Anal. Chem.* **2009**, *81*, 8426–8433.
[42] a) B. Prats Mateu, M. Felhofer, A. De Juan, N. Gierlinger, *Plant Methods* **2018**, *14*; b) J. Shlens, arXiv:1404.1100v1 **2014**.
[43] F. Bonnier, H. Byrne, *Analyst* **2011**, *137*, 322–332.
[44] U. Agarwal, R. S. Reiner, A. Pandey, S. A. Ralph, K. Hirth, R. H. Atalla, in *Appita Annual Conference*, *Vol. 3*, **2005**.
[45] P. Bock, P. Nousiainen, T. Elder, M. Blaukopf, H. Amer, R. Zirbs, A. Potthast, N. Gierlinger, *J. Raman Spectrosc.* **2020**, 51, 422–431..
[46] a) G. Neutelings, *Plant Sci.* **2011**, *181*, 379–386; b) J. Ralph, *Lignin structure: recent developments*, **2010**, Madison, WI: US Dairy Forage Research Center, USDA-Agricultural Research Service.
[47] A. Gómez-Sánchez, M. Marro, M. Marsal, S. Zacchetti, R. Rocha de Oliveira, P. Loza-Alvarez, A. de Juan, *Sci. Rep.* **2021**, *11*, 18665.
[48] P. H. C. Eilers, *Anal. Chem.* **2003**, *75*, 3631–3636.

Manuscript received: February 13, 2022
Revised manuscript received: May 9, 2022
Accepted manuscript online: May 11, 2022
Version of record online: June 1, 2022